Porous Polymer Materials

International Edition: DOI: 10.1002/anie.201503418
German Edition: DOI: 10.1002/ange.201503418

Thiophene, Selenophene, and Tellurophene-based Three-Dimensional Organic Frameworks**

*Peng-Fei Li, Tyler B. Schon, and Dwight S. Seferos**

Abstract: *3D frameworks are important because of their potential to combine the advantageous properties of porous materials with those associated with polymers. A series of novel 3D aromatic frameworks are presented that incorporate the heterocycles thiophene, selenophene, and tellurophene. The specific surface area and pore width of frameworks depends on the element that is used to build the framework. Optoelectronic properties are element-dependent, with heavy atoms red-shifting the optical properties and decreasing the energy gap of the solid. The metalloid nature of tellurophene allows the properties of this material to be tuned based on its oxidation state, even as an insoluble solid. The incorporation of the optoelectronic active thiophene, selenophene, and tellurophene units and the effect that they have on properties was studied. A supercapcitor device was fabricated using these frameworks, showing that these 3D frameworks are promising for optoelectronic uses.*

Materials such as activated carbon[1] and zeolites[2] are very important and have applications that range from chemical separation to drug delivery. Recently, novel porous materials with tunable pore width and function, such as metal–organic frameworks,[3] covalent organic frameworks,[4] and porous aromatic frameworks,[5] have emerged as promising candidates in many different areas. Aromatic frameworks in particular have received much interest because of their potential to combine the advantageous properties of both porous materials and polymers. Aromatic frameworks exhibit several advantages, including designable surface area and porosity, diversity of synthetic routes, and in certain cases post-synthetic chemical modification. Indeed, aromatic frameworks have found many different applications including gas adsorption,[6] energy storage,[7] and wastewater treatment.[8] However, few frameworks have properties that are appropriate for optoelectronics, even though they offer certain potential advantages, chiefly the ability to rationally design a complex organic solid.[9] The most common building block for optoelectronic materials, namely thiophene[10] and related heterocycles, have been nearly unexplored in this area, save one recently reported example of a 2D framework.[11] This thiophene framework was highly crystalline and had a large surface area. This prompted us to ask whether other heterocycles that are common to organic electronics may serve as building blocks for the preparation of porous frameworks. In particular, we are interested in 3D structures for which there are no examples that are composed of heterocycles. These 3D structures can be useful in a wider range of applications than the corresponding 2D materials.

Herein we report a series of novel 3D aromatic frameworks that incorporate the heterocycles thiophene, selenophene, and tellurophene. As mentioned previously, thiophene is perhaps the most common building block for organic electronic materials. More recently, heavier heterocycles have been employed and studied including selenophenes[12] and even tellurophenes.[13] The advantage of these heavier-homologue heterocycles include a more narrow HOMO–LUMO gap, greater polarizability, and the ability to exploit the unique reactivity of the heavy atoms, namely tellurium. Herein, we report the synthesis and characterization of 3D frameworks based on diphenylthiophene (**DPT**), diphenylselenophene (**DPSe**), and diphenyltellurophene (**DPTe**).

Thiophene, selenophene, and tellurophene-based 3D frameworks consist of adamantane vertices and diphenylheterocycle linkages. The structures of these 3D materials were first predicted by the semi-empirical geometry optimization of a separated cage (Supporting Information, Figures S1–S3). The ideal structure of frameworks with linear linkers is the diamond structure. However, **DPT**, **DPSe**, and **DPTe** are curved molecules, which results in a twisted structure (Figure 1). **DPTe** is the most linear building block in this series due to its long C–Te bond ($d_{C-Te} = 2.09$ Å compared to $d_{C-Se} = 1.90$ Å and $d_{C-S} = 1.75$ Å). As a result, the optimized structure of **Te-3D** is almost an ideal diamond (Supporting Information, Figure S3). All of the optimized structures have an inner sphere diameter of around 30 Å, which means that they are potential mesoporous materials (Figure 1).

The 3D frameworks were synthesized by a $[Pd(PPh_3)_4]$ catalyzed Stille coupling reaction between 1,3,5,7-tetrakis(4-iodophenyl)adamantane[14] and corresponding 2,5-bis(trimethyltin)heterocycles[15] in degassed DMF at 120 °C for 3 days. This reaction afforded green-brown powders of **S-3D**, **Se-3D**, and **Te-3D**. The solids were washed with acetone and chloroform to remove any residual starting material, and then transferred to a vial and activated under vacuum at 120 °C overnight (Figure 1). All of the afforded solids were insoluble in common solvents, such as acetone, chloroform, DMF, and water. Elemental analyses confirmed that the C and H content in all three solids are as similar to the

[*] Dr. P. F. Li, T. B. Schon, Prof. D. S. Seferos
Department of Chemistry, University of Toronto
80 St. George, Toronto, ON M5S 3H6 (Canada)
E-mail: dseferos@chem.utoronto.ca
Homepage: http://www.chem.utoronto.ca/wp/seferos/

[**] This work was supported by the National Science and Engineering Council of Canada and the Alfred P. Sloan Foundation. We thank Dr. Srebri Petrov and Dr. Abdolkarim Danaei for assistance with PXRD measurements.

Supporting information for this article is available on the WWW under http://dx.doi.org/10.1002/anie.201503418.

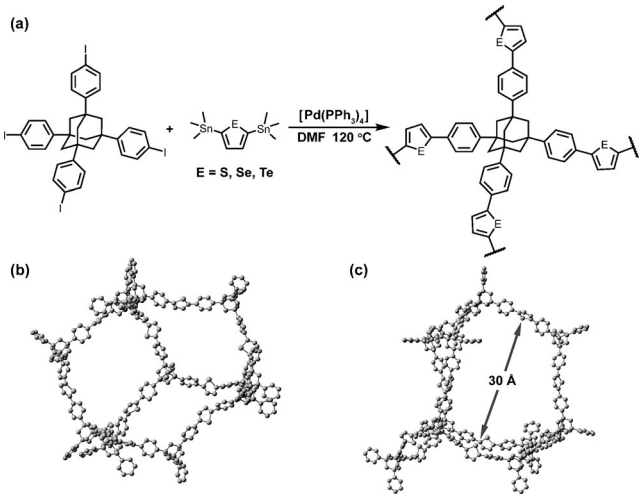

Figure 1. a) The synthesis of the 3D materials. b), c) Views of a representative geometry-optimized structure model of **Se-3D**. Hydrogen atoms are not shown for clarity.

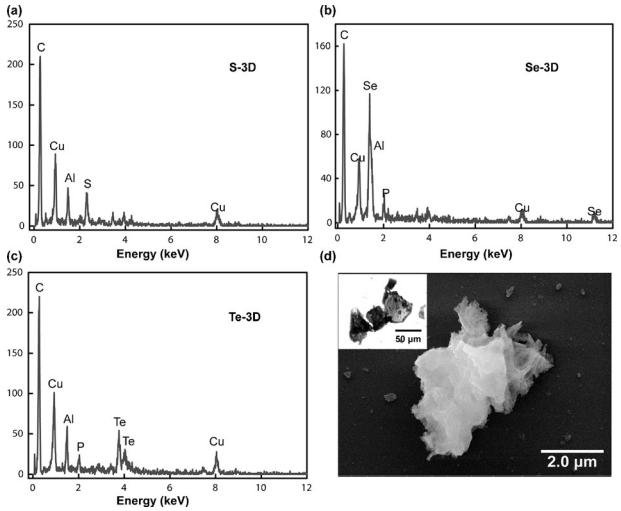

Figure 2. a)–c) EDX spectra of the frameworks and d) an SEM image of **Se-3D**. The inset of (d) shows a microscope image of **Se-3D**. Note that Al and Cu arise from the sample holder and grid, respectively.

theoretical value as those typically reported for frameworks (residual DMF may cause values to differ from those expected).[16] Comparing the IR spectra of frameworks with their starting materials indicates the attenuation of the methyl signal from trimethyltin group (2960 cm^{-1} and 1260 cm^{-1}). The appearance of the *para*-disubstituted benzene signal at 800–860 cm^{-1} and the heterocycle signal at about 1650 cm^{-1} indicates the presence of tetraphenyladamantane and heterocycle linkages (Supporting Information, Figures S4–S6). ^{13}C cross-polarization/magic-angle spinning (CP-MAS) NMR spectroscopy (Supporting Information, Figures S7–S9) reveals that **S-3D**, **Se-3D**, and **Te-3D** contain three types of aromatic carbon atoms (ranging from 126 to 150 ppm) and two types of aliphatic carbon atoms (around 41 and 48 ppm). All three frameworks are mostly amorphous as indicated by the powder X-ray measurements (Supporting Information, Figures S10–S12). **S-3D** and **Se-3D** exhibit no peaks in the diffraction pattern, which can be explained by their twisted structure resulting in an irregular framework (Figure 1; Supporting Information, Figure S1). **Te-3D** on the other hand exhibits weak peaks at 2.3 degree corresponding to a lattice spacing of 38.4 Å and this is the pore size estimated by modeling and BET measurements (Supporting Information, Figure S3). The weak peaks in **Te-3D** can be explained by the more ideal-like diamond structure that is due to the more co-linear tellurophene linker. Thermogravimetric analyses (TGAs) were conducted on activated samples of **S-3D**, **Se-3D**, and **Te-3D**. All of the samples lost guest solvent molecules upon heating to 150 °C, and started to decompose around 250 °C (Supporting Information, Figures S13–S15). All of the frameworks do contain defects, namely unreacted sites that contain residual $SnMe_3$ groups. A likely pathway of decomposition is the loss of these groups, and this is likely why each compound decomposes at roughly the same temperature.

Scanning electron microscopy (SEM) reveals that all frameworks are sheet-like (Figure 2d; Supporting Information, Figures S16–S17). Further characterization with energy-dispersive X-ray spectroscopy (EDX) reveals clear signals from S, Se, and Te in the corresponding samples (Figure 2a–c). The signal around 2 keV in **Se-3D** and **Te-3D** samples is P, which comes from the triphenylphosphine ligands from the catalyst. The small signal around 3–4 keV is either residual Sn from defect sites where linkages did not occur (described in more detail below) or Pd from the catalyst or both. Because these signals are very weak the exact assignment is difficult. The absence of I demonstrates high conversion of adamantine building block (within the detection limit of EDX) to the product. Different areas in each sample have similar elemental content, which shows the homogeneity of the material. The individual sheets of **Te-3D** are somewhat different than the other two frameworks. They are composed of smaller round plates with a circa 500 nm diameter (Supporting Information, Figure S18). The round plates have similar Te compositions, which shows their homogeneity (Supporting Information, Figures S19–S21). Microscope images reveal that all frameworks are transparent particles with different color, from light yellow to amber. The color gradually deepens with heavier elements (Supporting Information, Figures S22–S24).

The pore structure was evaluated by nitrogen sorption isotherms measured at 77 K. **S-3D** and **Se-3D** are mesoporous and exhibit type IV reversible sorption profiles (Figure 3; Supporting Information, Figures S25, S26). The BET (Brunauer–Emmett–Teller) specific surface area of **S-3D** is 537.2 $m^2 g^{-1}$ (Supporting Information, Figure S25). The pore size distribution of **S-3D** is broad and centered at 52 Å as estimated by density functional theory (DFT; Supporting Information, Figure S26). The larger-than-ideal pore size is due to missing linkages in the frameworks. **Se-3D** has a slightly decreased surface area of 478.8 $m^2 g^{-1}$ (Figure 3a). The pore size distribution of **Se-3D** is complex compared with **S-3D**. The first peak at 42 Å is close to the target porosity predicted by geometry optimization (Figure 1c, Figure 3b). The adjacent peak at about 76 Å is most likely due to defects in the frameworks, for example, a large pore from two merged small

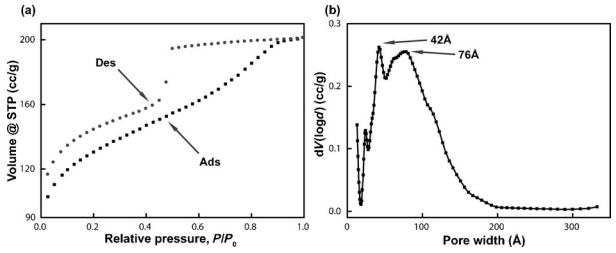

Figure 3. a) Nitrogen sorption isotherm of **Se-3D**, b) pore size distribution profile of **Se-3D**.

pores. The pore size distribution of **Te-3D** is similar to **Se-3D** and shows that some of the expected pores exist in this framework. The peak at 33 Å and small hysteresis in the isotherm indicates a potential mesoporous material (Supporting Information, Figures S27, S28). However the BET surface area of **Te-3D** is very low and cannot be explained by the heavier atom, alone. The drop in the surface area for **Te-3D** is most likely due to stronger Te–Te interactions[17] that lead to lower solubilty during synthesis and more interpenetraion in the solid state.

To elucidate the optoelectronic properties **S-3D**, **Se-3D**, and **Te-3D**, a series of DFT calculations were carried out. The geometry of model compounds **DPT**, **DPSe**, and **DPTe** were optimized using the Gaussian 09 software package at the B3LYP level of theory with the 6-31 + G(d) basis set for C, H, and S, and the LANL2DZ basis set for Se and Te. All geometries were optimized to a minimum as verified by frequency calculations. The heterocycles are non-planar with respect to their two adjacent phenyl rings in all three compounds (Supporting Information, Figures S29–S31). The diphenyl model represents the average geometry of the porous polymer, although the twisting angle likely varies in the porous framework (Figure 1). The diphenyl model was also used to estimate the frontier orbital levels. The HOMO levels gradually increase from **DPT** (−5.694 eV) to **DPSe** (−5.469 eV) to **DPTe** (−5.437 eV). The corresponding HOMO–LUMO gap also decreases slightly, from 4.027 to 3.977 eV, which is the expected trend for a Group 16 compound series.[18] All three models exhibit similar HOMO and LUMO level distributions (Supporting Information, Figures S29–S31). However the electron density on the center ring decreases with heavier element.

Additional experiments were conducted to better understand the optoelectronic properties of **S-3D**, **Se-3D**, and **Te-3D**. Since the materials are insoluble in water, a suspension was prepared by sonicating a mixture of the corresponding framework in distilled water. This resulted in homogeneous translucent solution that could be further studied. The optical absorption spectra of the suspensions were collected using an integrating sphere in transmission mode (Figure 4c). Similar to the solution UV/Vis of monomers (Supporting Information, Figure S44), the λ_{max} decreases in energy from **S-3D** to **Se-3D** to **Te-3D**. In fact, the λ_{max} of **Te-3D** is 366 nm, significantly red-shifted, which is consistent with the calculated HOMO–LUMO energy gap. We also investigated the excitation and emission spectra of **S-3D**, **Se-3D**, and **Te-3D. S-3D** exhibits strong fluorescence at 542 nm, while the emission

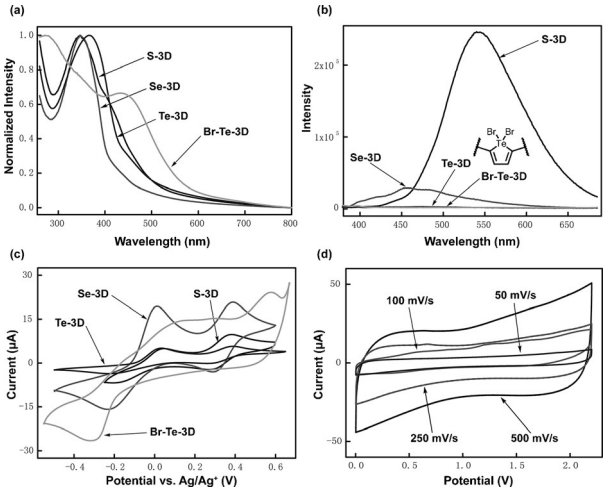

Figure 4. a) Suspension UV/Vis spectra of 3D frameworks in water, b) suspension fluorescence spectra of 3D frameworks, c) cyclic voltammetry of 3D frameworks, and d) cyclic voltammograms of the asymmetric supercapacitor based on **S-3D**.

of **Se-3D** is attenuated and appears broad with a maximum emission at 456 nm. **Te-3D** does not exhibit fluorescence, even with different excitation energies. This is consistent with the highly dense packing of the material and the heavy-element effect of tellurium.

To study the electrochemistry of this series of frameworks, cyclic voltammograms were collected on their thin films on Pt electrodes. We fabricated these films with 50 wt % poly(vinylidene fluoride-*co*-hexafluoropropylene) (PVDF-*co*-HFP) to give robust, homogenous films. All three 3D frameworks exhibit two redox waves (Figure 4c; Supporting Information, Figure S36–S38). The first redox wave of all three frameworks has a large peak splitting (ca. 200 mV) and an equal magnitude of current for anodic and cathodic peaks. The second redox wave has a peak splitting around 100 mV and is more reversible compared with the first peak. All frameworks have similar half-wave potentials ranging from −0.08 to −0.11 V for the first and 0.33 to 0.34 V for the second (Supporting Information, Table S2). We note that from DFT predictions, **Se-3D** and **Te-3D** should have a similar oxidation potential, whereas **S-3D** should be different. There are several possible reasons why the experimental oxidation potentials are different from the trends predicted by DFT. The oxidation potential can be influenced by the material properties and CV measurement conditions. The frameworks have different porosities and different micro environments, which is difficult to model. Also the calculations are performed in the gas phase. This does not take into account any interactions the heterocycle may have with the electrolyte or the intermolecular interactions that could result.

The presence of two redox waves can be explained by several possible factors, such as the different chemical environment of the outer and inner framework, and also conformational changes within the framework. The presence of defects, however, are the most likely cause of these two peaks. Defects occur during the synthesis. The synthesis of the framework requires that the connections are built by coupling

reactions between one heterocycle and two phenyl-substituted adamantane cages. If only one phenyl-substituted adamantane cage is coupled to the heterocycle, it leads to a defect. The defects were modeled as mono-substituted phenyl heterocycles (**PT**, **PSe**, and **PTe**). These model defects have a lower lying HOMO levels and are therefore expected to be more difficult to oxidize (Supporting Information, Table S1 and Figures S33–S35). This modeling study provides an explanation for the interesting experimental observation that the frameworks undergo more than one oxidation event. Namely, the first is centered on the fully formed linkage, while the second is centered on the defect site with only one phenyl group. Unfortunately we have not been able fully eliminate defects by altering the synthesis. It is also difficult to know the exact ratio of defects to fully coupled heterocycles by examining the CV owing to the possibility of electrical isolation of the inner most redox sites in a framework, especially if the individual frameworks are large.

Our group has shown that the metalloid nature of tellurophene leads to new ways of controlling optoelectronic properties. Tellurophene forms a coordination complex with halogens including molecular bromine where one equivalent of Br_2 adds to Te.[13a,15e,19] This leads to significant changes in the optoelectronic properties. To test if this would be the case in an insoluble framework, bromine was added to **Te-3D** in chloroform, and stirred overnight under argon in the dark. The color of the powder changes from green-brown to orange-red, indicating that a reaction has taken place. Optical spectroscopy reveals that the λ_{max} of **Br-Te-3D** significantly red shifts to 441 nm, compared with the λ_{max} of **Te-3D** at 366 nm. This is also consistent with the calculated HOMO–LUMO energy gap on that structure (Supporting Information, Figure S32 and Table S1). Cyclic voltammetry reveals that **Br-Te-3D** exhibits an irreversible redox process (Figure 4c; Supporting Information, Figure S39). Compared with **Te-3D**, the first cathodic peak E_{pc1} is shifted negatively. This is in agreement with the reduced band gap observed by UV/Vis spectroscopy. The addition of bromine causes a significant change the binding energy of the tellurium core (from X-ray photoelectron spectroscopy), from 574.06 to 576.96 eV (Supporting Information, Figures S40, S41). This shows that these frameworks are dynamic and can be altered based on their oxidation state.

As a demonstration of the applicability of this class of material in an organic electronic device, an asymmetric supercapacitor was constructed using **S-3D** as the positive electrode and carbon black as the negative electrode. The device exhibits a pseudo-rectangular cyclic voltammogram, indicative of the pseudocapacitive nature of the **S-3D** electrode (Figure 4d; Supporting Information, Figure S42). The device has an areal capacitance of $4.01 \pm 0.05\ mF\,cm^{-2}$ at a current density of $0.1\ A\,g^{-1}$. Importantly, these devices appear to be quite stable. After 500 cycles, the peak current is still 80% of the initial value (Supporting Information, Figure S43). Moreover, loss of current only takes place in the initial cycles and current decays very slowly thereafter. This slow decay after the initial decrease demonstrates the stability of the material with respect to cycling, which is most likely due to its ability to accommodate ions with its porosity and its stability towards solvents. The capacitance of the device falls slightly lower than previous reports (typical values range from 6–90 $mF\,cm^{-2}$);[20] however these values are for areal capacitance, which are highly dependent on the thickness of the electrode, and can be further improved by having thicker films. Capacitance can also be improved by optimizing the electrode fabrication, device fabrication, tuning the pore size, and by using a redox active material on the negative electrode.

In summary, the first series of all of the stable group-16-containing heterocycle frameworks (S, Se, and Te) have now been synthesized and characterized. These materials are thermally stable up to 250 °C. The specific surface area and porewidth of frameworks depends on the Group 16 element incorporated in the heterocycle. The optoelectronic properties are element-dependent with heavy atoms red-shifting the optical properties and decreasing the oxidation potential. The metalloid nature of tellurophene allows this material to be oxidized, even as an insoluble solid. Significant changes to the optotelectronic properties and core electron binding energy are affected by framework oxidation. The incorporation of optoelectronically active thiophene, selenophene and tellurophene, and the dynamic nature of tellurophene, make this series of material promising candidates for optoelectronic uses. The applicability of these materials has been demonstrated by constructing an asymmetric supercapacitor using **S-3D**. The device exhibits a low capacitance; however, the stability of the material highlights the advantages of the use of these 3D mesoporous organic frameworks in organic electronics.

Keywords: 3D frameworks · porous materials · selenophene · tellurophene · thiophene

How to cite: *Angew. Chem. Int. Ed.* **2015**, *54*, 9361–9366
Angew. Chem. **2015**, *127*, 9493–9498

[1] J. W. Patrick, *Porosity in Carbons: Characterization and Applications*, Wiley, London, **1995**.

[2] a) A. Corma, *Chem. Rev.* **1997**, *97*, 2373–2420; b) J. Cejka, H. von Bekkum, A. Corma, F. Schüth, *Introduction to Zeolite Science and Practice*, *3rd ed.*, Elsevier, Amsterdam, **2007**; c) R. Xu, W. Pang, J. Yu, Q. Huo, J. Chen, *Chemistry of Zeolites and Related Porous Materials: Synthesis and Structure*, Wiley, New York, **2007**; d) H. Qi, X. Roy, K. E. Shopsowitz, J. K. H. Hui, M. J. MacLachlan, *Angew. Chem. Int. Ed.* **2010**, *49*, 9740–9743; *Angew. Chem.* **2010**, *122*, 9934–9937; e) K. E. Shopsowitz, H. Qi, W. Y. Hamad, M. J. MacLachlan, *Nature* **2010**, *468*, 422–425; f) K. E. Shopsowitz, W. Y. Hamad, M. J. MacLachlan, *Angew. Chem. Int. Ed.* **2011**, *50*, 10991–10995; *Angew. Chem.* **2011**, *123*, 11183–11187; g) K. E. Shopsowitz, W. Y. Hamad, M. J. MacLachlan, *J. Am. Chem. Soc.* **2011**, *133*, 867–870; h) M. K. Khan, M. Giese, M. Yu, J. A. Kelly, W. Y. Hamad, M. J. MacLachlan, *Angew. Chem. Int. Ed.* **2013**, *52*, 8921–8924; *Angew. Chem.* **2013**, *125*, 9089–9092; i) J. A. Kelly, M. Giese, K. E. Shopsowitz, W. Y. Hamad, M. J. MacLachlan, *Acc. Chem. Res.* **2014**, *47*, 1088–1096.

[3] a) O. M. Yaghi, M. O'Keeffe, N. W. Ockwig, H. K. Chae, M. Eddaoudi, J. Kim, *Nature* **2003**, *423*, 705–714; b) M. O'Keeffe, M. A. Peskov, S. J. Ramsden, O. M. Yaghi, *Acc. Chem. Res.* **2008**, *41*, 1782–1789; c) J. An, S. J. Geib, N. L. Rosi, *J. Am. Chem. Soc.* **2009**, *131*, 38–39; d) O. K. Farha, J. T. Hupp, *Acc. Chem. Res.*

2010, *43*, 1166 – 1175; e) J. An, N. L. Rosi, *J. Am. Chem. Soc.* **2010**, *132*, 5578 – 5579; f) I. Imaz, M. Rubio-Martinez, J. An, I. Sole-Font, N. L. Rosi, D. Maspoch, *Chem. Commun.* **2011**, *47*, 7287 – 7302; g) J. An, O. K. Farha, J. T. Hupp, E. Pohl, J. I. Yeh, N. L. Rosi, *Nat. Commun.* **2012**, *3*, 604; h) V. N. Vukotic, K. J. Harris, K. Zhu, R. W. Schurko, S. J. Loeb, *Nat. Chem.* **2012**, *4*, 456 – 460; i) V. N. Vukotic, S. J. Loeb, *Chem. Soc. Rev.* **2012**, *41*, 5896 – 5906; j) N. B. Shustova, A. F. Cozzolino, M. Dincă, *J. Am. Chem. Soc.* **2012**, *134*, 19596 – 19599; k) N. B. Shustova, A. F. Cozzolino, S. Reineke, M. Baldo, M. Dincă, *J. Am. Chem. Soc.* **2013**, *135*, 13326 – 13329; l) A. Foucault-Collet, K. A. Gogick, K. A. White, S. Villette, A. Pallier, G. Collet, C. Kieda, T. Li, S. J. Geib, N. L. Rosi, S. Petoud, *Proc. Natl. Acad. Sci. USA* **2013**, *110*, 17199 – 17204; m) T. Li, D.-L. Chen, J. E. Sullivan, M. T. Kozlowski, J. K. Johnson, N. L. Rosi, *Chem. Sci.* **2013**, *4*, 1746 – 1755; n) Z. Xie, T. Li, N. L. Rosi, M. A. Carreon, *J. Mater. Chem. A* **2014**, *2*, 1239 – 1241; o) K. Zhu, V. N. Vukotic, C. A. O'Keefe, R. W. Schurko, S. J. Loeb, *J. Am. Chem. Soc.* **2014**, *136*, 7403 – 7409.

[4] a) M. Mastalerz, *Angew. Chem. Int. Ed.* **2008**, *47*, 445 – 447; *Angew. Chem.* **2008**, *120*, 453 – 455; b) D. Jiang, X. Ding, J. Guo in *Supramolecular Soft Matter: Applications in Materials and Organic Electronics* (Ed.: T. Nakanishi), Wiley, Hoboken, **2011**; c) X. Feng, X. Ding, D. Jiang, *Chem. Soc. Rev.* **2012**, *41*, 6010 – 6022; d) S.-Y. Ding, W. Wang, *Chem. Soc. Rev.* **2013**, *42*, 548 – 568.

[5] a) N. B. McKeown, P. M. Budd, K. J. Msayib, B. S. Ghanem, H. J. Kingston, C. E. Tattershall, S. Makhseed, K. J. Reynolds, D. Fritsch, *Chem. Eur. J.* **2005**, *11*, 2610 – 2620; b) N. B. McKeown, P. M. Budd, *Chem. Soc. Rev.* **2006**, *35*, 675 – 683; c) A. Thomas, P. Kuhn, J. Weber, M.-M. Titirici, M. Antonietti, *Macromol. Rapid Commun.* **2009**, *30*, 221 – 236; d) D. Wu, F. Xu, B. Sun, R. Fu, H. He, K. Matyjaszewski, *Chem. Rev.* **2012**, *112*, 3959 – 4015; e) D. Jiang, S. Jin, Y. Xu, X. Liu in *Nanoporous Materials: Synthesis and Applications* (Ed.: Q. Xu), Taylor & Francis Books, New York, **2013**; f) Y. Xu, S. Jin, H. Xu, A. Nagai, D. Jiang, *Chem. Soc. Rev.* **2013**, *42*, 8012 – 8031.

[6] a) J.-X. Jiang, F. Su, A. Trewin, C. D. Wood, N. L. Campbell, H. Niu, C. Dickinson, A. Y. Ganin, M. J. Rosseinsky, Y. Z. Khimyak, A. I. Cooper, *Angew. Chem. Int. Ed.* **2007**, *46*, 8574 – 8578; *Angew. Chem.* **2007**, *119*, 8728 – 8732; b) J.-X. Jiang, F. Su, A. Trewin, C. D. Wood, H. Niu, J. T. A. Jones, Y. Z. Khimyak, A. I. Cooper, *J. Am. Chem. Soc.* **2008**, *130*, 7710 – 7720; c) T. Ben, H. Ren, S. Ma, D. Cao, J. Lan, X. Jing, W. Wang, J. Xu, F. Deng, J. M. Simmons, S. Qiu, G. Zhu, *Angew. Chem. Int. Ed.* **2009**, *48*, 9457 – 9460; *Angew. Chem.* **2009**, *121*, 9621 – 9624; d) W. Lu, D. Yuan, D. Zhao, C. I. Schilling, O. Plietzsch, T. Muller, S. Bräse, J. Guenther, J. Blümel, R. Krishna, Z. Li, H.-C. Zhou, *Chem. Mater.* **2010**, *22*, 5964 – 5972; e) C. Zhang, Y. Liu, B. Li, B. Tan, C.-F. Chen, H.-B. Xu, X.-L. Yang, *ACS Macro Lett.* **2011**, *1*, 190 – 193; f) A. Comotti, S. Bracco, M. Mauri, S. Mottadelli, T. Ben, S. Qiu, P. Sozzani, *Angew. Chem. Int. Ed.* **2012**, *51*, 10136 – 10140; *Angew. Chem.* **2012**, *124*, 10283 – 10287; g) C. Zhang, J.-J. Wang, Y. Liu, H. Ma, X.-L. Yang, H.-B. Xu, *Chem. Eur. J.* **2013**, *19*, 5004 – 5008; h) L.-H. Xie, M. P. Suh, *Chem. Eur. J.* **2013**, *19*, 11590 – 11597; i) B. Li, Y. Zhang, R. Krishna, K. Yao, Y. Han, Z. Wu, D. Ma, Z. Shi, T. Pham, B. Space, J. Liu, P. K. Thallapally, J. Liu, M. Chrzanowski, S. Ma, *J. Am. Chem. Soc.* **2014**, *136*, 8654 – 8660.

[7] a) G. M. Suppes, B. A. Deore, M. S. Freund, *Langmuir* **2007**, *23*, 1064 – 1069; b) M. E. Roberts, D. R. Wheeler, B. B. McKenzie, B. C. Bunker, *J. Mater. Chem.* **2009**, *19*, 6977 – 6979; c) Y. Kou, Y. Xu, Z. Guo, D. Jiang, *Angew. Chem. Int. Ed.* **2011**, *50*, 8753 – 8757; *Angew. Chem.* **2011**, *123*, 8912 – 8916; d) S. Chen, J. Duan, Y. Tang, S. Zhang Qiao, *Chem. Eur. J.* **2013**, *19*, 7118 – 7124; e) L. Zhang, F. Zhang, X. Yang, G. Long, Y. Wu, T. Zhang, K. Leng, Y. Huang, Y. Ma, A. Yu, Y. Chen, *Sci. Rep.* **2013**, *3*, 1408; f) D. Puthusseri, V. Aravindan, S. Madhavi, S. Ogale, *Energy Environ. Sci.* **2014**, *7*, 728 – 735; g) F. Xu, X. Chen, Z. Tang, D. Wu, R. Fu, D. Jiang, *Chem. Commun.* **2014**, *50*, 4788 – 4790.

[8] B. Li, Y. Zhang, D. Ma, Z. Shi, S. Ma, *Nat. Commun.* **2014**, *5*, 5537.

[9] a) M. Calik, F. Auras, L. M. Salonen, K. Bader, I. Grill, M. Handloser, D. D. Medina, M. Dogru, F. Löbermann, D. Trauner, A. Hartschuh, T. Bein, *J. Am. Chem. Soc.* **2014**, *136*, 17802 – 17807; b) L. Chen, K. Furukawa, J. Gao, A. Nagai, T. Nakamura, Y. Dong, D. Jiang, *J. Am. Chem. Soc.* **2014**, *136*, 9806 – 9809.

[10] a) G. Li, V. Shrotriya, J. Huang, Y. Yao, T. Moriarty, K. Emery, Y. Yang, *Nat. Mater.* **2005**, *4*, 864 – 868; b) W. Ma, C. Yang, X. Gong, K. Lee, A. J. Heeger, *Adv. Funct. Mater.* **2005**, *15*, 1617 – 1622; c) Y. Kim, S. Cook, S. M. Tuladhar, S. A. Choulis, J. Nelson, J. R. Durrant, D. D. C. Bradley, M. Giles, I. McCulloch, C.-S. Ha, M. Ree, *Nat. Mater.* **2006**, *5*, 197 – 203; d) Y.-J. Cheng, C.-H. Hsieh, Y. He, C.-S. Hsu, Y. Li, *J. Am. Chem. Soc.* **2010**, *132*, 17381 – 17383; e) J. Hollinger, A. A. Jahnke, N. Coombs, D. S. Seferos, *J. Am. Chem. Soc.* **2010**, *132*, 8546 – 8547.

[11] G. H. V. Bertrand, V. K. Michaelis, T.-C. Ong, R. G. Griffin, M. Dincă, *Proc. Natl. Acad. Sci. USA* **2013**, *110*, 4923 – 4928.

[12] a) L. Li, J. Hollinger, A. A. Jahnke, S. Petrov, D. S. Seferos, *Chem. Sci.* **2011**, *2*, 2306 – 2310; b) L. Li, J. Hollinger, N. Coombs, S. Petrov, D. S. Seferos, *Angew. Chem. Int. Ed.* **2011**, *50*, 8148 – 8152; *Angew. Chem.* **2011**, *123*, 8298 – 8302; c) D. Gao, J. Hollinger, D. S. Seferos, *ACS Nano* **2012**, *6*, 7114 – 7121; d) J. Hollinger, D. S. Seferos, *Macromolecules* **2014**, *47*, 5002 – 5009; e) H. Yan, J. Hollinger, C. R. Bridges, G. R. McKeown, T. Al-Faouri, D. S. Seferos, *Chem. Mater.* **2014**, *26*, 4605 – 4611.

[13] a) A. A. Jahnke, G. W. Howe, D. S. Seferos, *Angew. Chem. Int. Ed.* **2010**, *49*, 10140 – 10144; *Angew. Chem.* **2010**, *122*, 10338 – 10342; b) A. A. Jahnke, D. S. Seferos, *Macromol. Rapid Commun.* **2011**, *32*, 943 – 951; c) Y. S. Park, Q. Wu, C.-Y. Nam, R. B. Grubbs, *Angew. Chem. Int. Ed.* **2014**, *53*, 10691 – 10695; *Angew. Chem.* **2014**, *126*, 10867 – 10871; d) Y. S. Park, T. S. Kale, C. Y. Nam, D. Choi, R. B. Grubbs, *Chem. Commun.* **2014**, *50*, 7964 – 7967; e) G. He, W. Torres Delgado, D. J. Schatz, C. Merten, A. Mohammadpour, L. Mayr, M. J. Ferguson, R. McDonald, A. Brown, K. Shankar, E. Rivard, *Angew. Chem. Int. Ed.* **2014**, *53*, 4587 – 4591; *Angew. Chem.* **2014**, *126*, 4675 – 4679; f) G. He, B. D. Wiltshire, P. Choi, A. Savin, S. Sun, A. Mohammadpour, M. J. Ferguson, R. McDonald, S. Farsinezhad, A. Brown, K. Shankar, E. Rivard, *Chem. Commun.* **2015**, *51*, 5444 – 5447.

[14] a) H. Newman, *Synthesis* **1972**, 692 – 693; b) E. B. Merkushev, N. D. Simakhina, G. M. Koveshnikova, *Synthesis* **1980**, 486 – 487; c) L. J. Mathias, V. R. Reichert, A. V. G. Muir, *Chem. Mater.* **1993**, *5*, 4 – 5; d) V. R. Reichert, L. J. Mathias, *Macromolecules* **1994**, *27*, 7015 – 7023.

[15] a) D. P. Sweat, C. E. Stephens, *J. Organomet. Chem.* **2008**, *693*, 2463 – 2464; b) D. P. Sweat, C. E. Stephens, *Synthesis* **2009**, 3214 – 3218; c) T. Earmme, Y.-J. Hwang, N. M. Murari, S. Subramaniyan, S. A. Jenekhe, *J. Am. Chem. Soc.* **2013**, *135*, 14960 – 14963; d) Y. Kim, J. Hong, J. H. Oh, C. Yang, *Chem. Mater.* **2013**, *25*, 3251 – 3259; e) E. I. Carrera, T. M. McCormick, M. J. Kapp, A. J. Lough, D. S. Seferos, *Inorg. Chem.* **2013**, *52*, 13779 – 13790.

[16] For typical deviations in elemental analyses, see: a) Ref. [6d]; b) E. L. Spitler, W. R. Dichtel, *Nat. Chem.* **2010**, *2*, 672 – 677; c) X. Ding, J. Guo, X. Feng, Y. Honsho, J. Guo, S. Seki, P. Maitarad, A. Saeki, S. Nagase, D. Jiang, *Angew. Chem. Int. Ed.* **2011**, *50*, 1289 – 1293; *Angew. Chem.* **2011**, *123*, 1325 – 1329. The residual DMF would be the reason for deviation in this case owing to its low volatility.

[17] a) J.-M. Chen, B. K. Santra, C. W. Liu, *Inorg. Chem. Commun.* **2004**, *7*, 1103 – 1105; b) M. Bühl, F. R. Knight, A. Křístková, I. Malkin Ondík, O. L. Malkina, R. A. M. Randall, A. M. Z.

Slawin, J. D. Woollins, *Angew. Chem. Int. Ed.* **2013**, *52*, 2495 – 2498; *Angew. Chem.* **2013**, *125*, 2555 – 2558; c) X.-Y. Wang, W. Jiang, T. Chen, H.-J. Yan, Z.-H. Wang, L.-J. Wan, D. Wang, *Chem. Commun.* **2013**, *49*, 1829 – 1831.

[18] a) G. L. Gibson, T. M. McCormick, D. S. Seferos, *J. Am. Chem. Soc.* **2012**, *134*, 539 – 547; b) T. M. McCormick, A. A. Jahnke, A. J. Lough, D. S. Seferos, *J. Am. Chem. Soc.* **2012**, *134*, 3542 – 3548; c) G. He, L. Kang, W. Torres Delgado, O. Shynkaruk, M. J. Ferguson, R. McDonald, E. Rivard, *J. Am. Chem. Soc.* **2013**, *135*, 5360 – 5363.

[19] E. I. Carrera, D. S. Seferos, *Dalton Trans.* **2015**, *44*, 2092 – 2096.

[20] a) A. Sumboja, C. Y. Foo, X. Wang, P. S. Lee, *Adv. Mater.* **2013**, *25*, 2809 – 2815; b) D. E. Shen, L. A. Estrada, A. M. Österholm, D. H. Salazar, A. L. Dyer, J. R. Reynolds, *J. Mater. Chem. A* **2014**, *2*, 7509 – 7516.

Received: April 15, 2015
Revised: May 8, 2015
Published online: June 19, 2015

